JOURNAL OF GEOPHYSICAL RESEARCH, VOL. 112, B06101, doi:10.1029/2006JB004548, 2007

Seismic imaging of the three-dimensional architecture of the Çınarcık Basin along the North Anatolian Fault

H. Carton,[1] S. C. Singh,[1] A. Hirn,[2] S. Bazin,[1] B. de Voogd,[3] A. Vigner,[2] A. Ricolleau,[1] S. Cetin,[4] N. Oçakoğlu,[5] F. Karakoç,[4] and V. Sevilgen[4,5]

Received 6 June 2006; revised 4 January 2007; accepted 8 March 2007; published 21 June 2007.

[1] The Çınarcık Basin is a transtensional basin located along the northern branch of the northern North Anatolian Fault (NAF) in the Sea of Marmara, the eastern half of which has been identified as a seismic gap. During the SEISMARMARA (2001) experiment, a dense grid of multichannel seismic reflection profiles was shot, covering the whole Çınarcık Basin and its margins. The new seismic images provide a nearly three-dimensional view of the architecture of the basin (fault system at depth and sedimentary infill) and provide insight into its tectonic evolution. Along both northern and southern margins of the basin, seismic reflection data show deep-penetrating faults, hence long-lived features, which have accommodated a large amount of extension. There is no indication in the data for a single throughgoing strike-slip fault, neither a cross-basin fault nor a pure strike-slip fault running along the northern margin. Faster opening is presently observed in the eastern part of the basin. The Çınarcık Basin seems to have developed as a transtensional basin across strike-slip segments of the northern NAF for the last few million years.

Citation: Carton, H., et al. (2007), Seismic imaging of the three-dimensional architecture of the Çınarcık Basin along the North Anatolian Fault, *J. Geophys. Res.*, *112*, B06101, doi:10.1029/2006JB004548.

1. Introduction

[2] The North Anatolian Fault (NAF) is a right-lateral strike-slip fault forming the plate boundary between Eurasia and Anatolia. It extends over 1600 km between the Karliova triple junction (Eurasia-Anatolia-Arabia triple junction) in the east and mainland Greece in the west (Figure 1, inset). The fault trace, which is well-defined in the topography across eastern and central Turkey, is close to a small circle. The best fitting Euler pole of rotation describing Anatolia/Eurasia motion is located in the Nile delta [*McClusky et al.*, 2000], at 30.7 ± 0.8°N, 32.6 ± 0.4°E, with an associated slip rate of about 24 mm/yr, deduced from analysis of Global Positioning System (GPS) data. In western Turkey, the NAF splits into two main strands called northern and southern NAF, with the northern branch carrying about 80 % of the displacement. The width of the deformation zone thus reaches 130 km in the Marmara area [*Barka and Kadinsky-Cade*, 1988]. Farther to the west, the NAF continues into the Aegean Sea where it interacts with Hellenic back-arc extension. Between 1939 and 1999, the linear part of the NAF ruptured in a sequence of westward-propagating earthquakes [e.g., *Stein et al.*, 1997; *Reilinger et al.*, 2000], the latest events being the İzmit and Duzce earthquakes in 1999. The eastern half of the Sea of Marmara is presently the site of a slip deficit [e.g., *Parsons*, 2004; *Pondard et al.*, 2007]. The importance of the seismic hazard to the neighboring city of Istanbul has created a high level of interest among the scientific community for a better understanding of the formation and tectonic evolution of the Sea of Marmara together with identification of major seismogenic faults at sea.

[3] The Sea of Marmara is a marine basin located south of Istanbul, with a broad, shallow shelf to the south and a deep northern part (Figure 1). The northern part (north Marmara trough, 160 km long) comprises three subbasins with up to 1250 m water depth, called from west to east the Tekirdağ, Central, and Çınarcık basins, and separated by topographic highs, the Western and Central highs. In the Anatolia/Eurasia rotation frame, the north Marmara trough is located at a left-stepping (extensional) jog of the northern branch of the NAF, between the strike-slip İzmit and Ganos segments, and is the site of active faulting and subsidence. However, the relationship between the Marmara basin and the NAF and the nature of the present-day tectonic activity have been a matter of debate. For a long time, available bathymetric and seismic reflection data were insufficient to construct a detailed and precise map of the

[1]Equipe de Géosciences Marines, Institut de Physique du Globe de Paris, Paris, France.
[2]Equipe de Sismologie, Institut de Physique du Globe de Paris, Paris, France.
[3]Département Sciences de la Terre, Université de Pau, Pau, France.
[4]TUBITAK-MAM, Marmara Research Center, Gebze-Kocaeli, Turkey.
[5]Department of Geophysics, Istanbul Technical University, Istanbul, Turkey.

0148-0227/07/2006JB004548$09.00

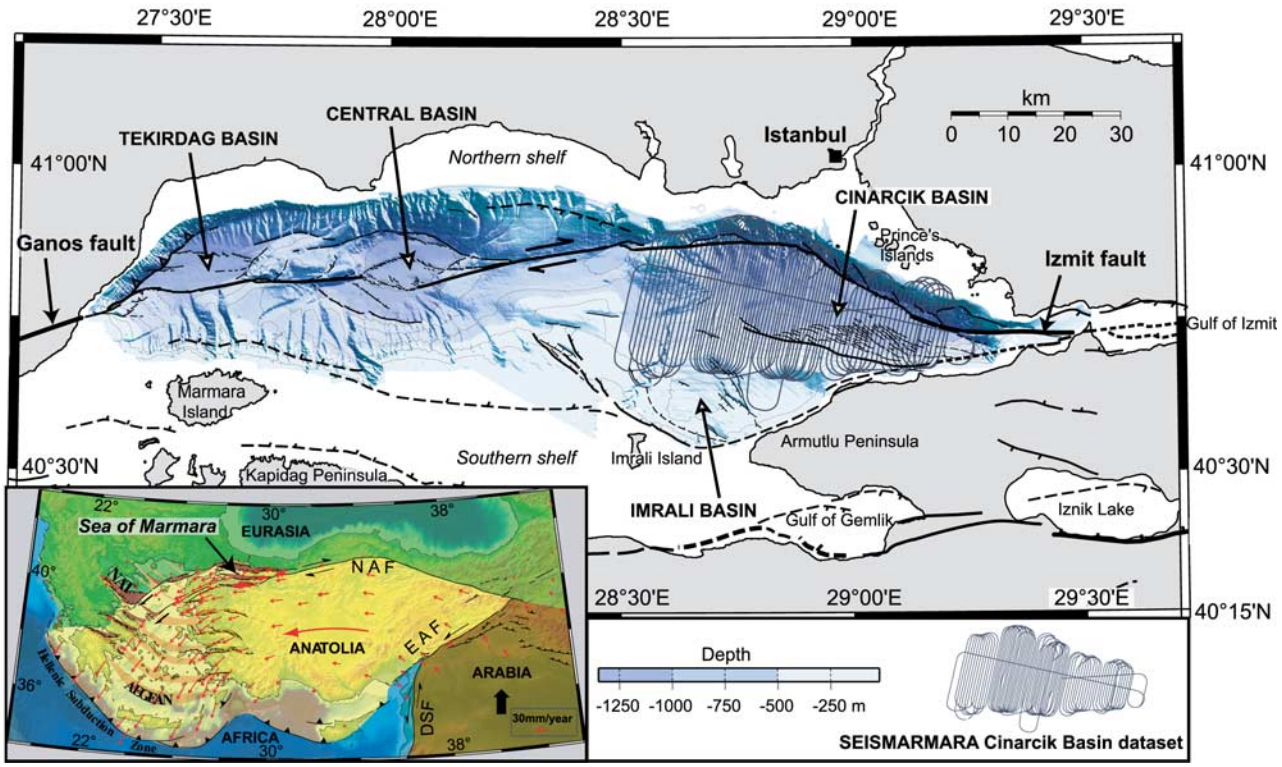

Figure 1. Location of the SEISMARMARA Çınarcık Basin (Leg 2) dataset superimposed on bathymetric map of the northern Sea of Marmara and fault system from *Armijo et al.* [2002]. The Çınarcık Basin is the easternmost and largest of three deep transtensional basins that have formed along the northern branch of the North Anatolian Fault. Inset (modified from *Armijo et al.* [2005]) shows tectonic setting of continental extrusion in eastern Mediterranean: the Anatolia-Aegea block escapes westward from the Arabia-Eurasis collision zone, towards the Hellenic subduction zone; small red arrows indicate GPS velocity vectors. NAF, North Anatolian Fault; EAF, East Anatolian Fault; DSF, Dead Sea fault.

active faults at sea, but the idea that the Sea of Marmara evolved as a (still active) pull-apart basin along the NAF [*Barka and Kadinsky-Cade*, 1988] was adopted by many authors [*Westaway*, 1994; *Smith et al.*, 1995; *Wong et al.*, 1995; *Ergün and Özel*, 1995; *Armijo et al.*, 1999]. An alternative view suggested that the Sea of Marmara deforms under the same influence as the geographically close Aegean [*Parke et al.*, 2002], a region where Hellenic back-arc extension has been active since 10–25 My. After the 1999 İzmit earthquake, a debate was initiated about the location, the nature of active fault strands in the Sea of Marmara, and the level of segmentation and slip partitioning, on which depends the magnitude of future events. Indeed, a single continuous strike-slip fault cutting across the whole basin [*Le Pichon et al.*, 2001] would produce a larger earthquake than an individual, smaller segment of a complex, segmented fault system, as proposed by other workers [*Okay et al.*, 2000; *Parke et al.*, 2002; *Armijo et al.*, 2002].

[4] This study focuses on the easternmost Çınarcık Basin (Figure 2), which from surface morphology appears as a wedge-shaped transtensional basin formed across a large releasing step-over in the main strike-slip fault zone [*Armijo et al.*, 2002]. Its sedimentary infill is likely to consist of Pliocene-Quaternary synkinematic sediments, at least 4 km thick [*Okay et al.*, 2000]. However, the stratigraphic control is poor since there has been no well drilled in the basin itself, and the closest available well data are from the MARMARA 1 borehole on the southern shelf [*Ergün and Özel*, 1995]. Apart from a few petroleum lines shown by *Ates et al.* [2003], previously published and interpreted seismic data [*Okay et al.*, 2000; *Parke et al.*, 1999, 2002; *İmren et al.*, 2001] could not image basin sediments deeper than the first water bottom multiple. In 2001, a combined multichannel seismics and Ocean Bottom Seismometer (OBS) experiment (SEISMARMARA) was carried out as a French-Turkish collaboration in order to study the crustal structure of the Sea of Marmara and to image the active faults at depth and the architecture of the deep basins. As part of this experiment, a grid of profiles at 600–900 m spacing was shot across the Çınarcık Basin and its margins, providing seismic images for the first 1 to 6 km of the subsurface. Results presented in this article include selected interpreted seismic profiles and sedimentary thickness maps. The new images provide insight into the three-dimensional structure (fault system at depth and sedimentary infill) and tectonic evolution of the Çınarcık Basin. The work presented here essentially focuses on the dip-slip component of the basin faults, which is easiest to assess from the seismic profiles. Interpretation was carried out by merging the processed profiles with existing data from an earlier survey [*Parke et al.*, 2003], available through the Incorporated Research Institutions for Seismology (IRIS) data repository. Extensive use of the high-resolution bathymetric data from the 2000 MARMARA cruise and subsequently published

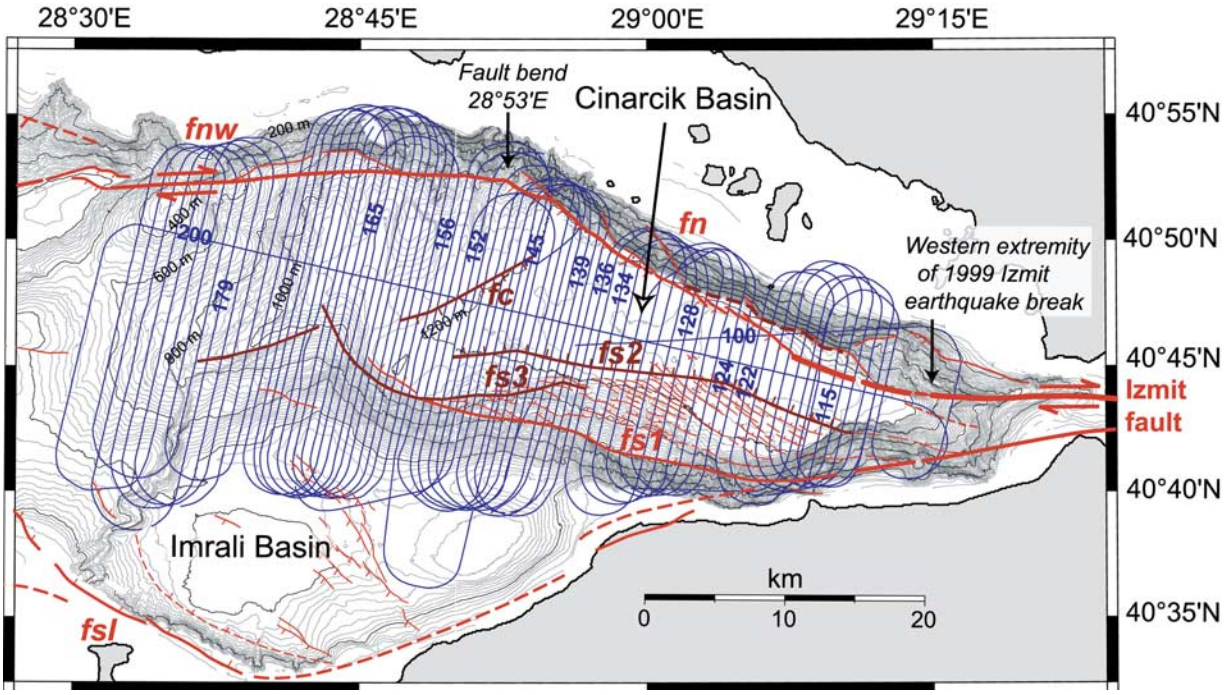

Figure 2. Fault map for the eastern Sea of Marmara modified after *Armijo et al.* [2002] (see fault names in Figure 3) and location of interpreted seismic profiles (this study) from the SEISMARMARA Çınarcık Basin grid. Faults marked in red are from Armijo et al., whereas in brown-red are indicated additional faults mapped on the basis of seismic data. Bathymetric contours every 20 m (thin grey lines) and every 200 m from 200 to 1200 m (thick black lines).

fault maps [*Le Pichon et al.*, 2001; *Armijo et al.*, 2002] was also made throughout this study.

2. Surface Morphology and Seismicity Pattern of the Çınarcık Basin

2.1. Surface Morphology

[5] The Çınarcık Basin is a wedge-shaped basin oriented N110°E, about 50 km long and up to 15–18 km wide, with a maximum seafloor depth of 1270 m (Figures 1 and 2). It considerably narrows eastward where it meets the Gulf of İzmit; it is bounded on its north and south sides by large topographic escarpments and to the west by a topographic high which isolates it from the Central Basin. Numerous canyons (generally N-S) cut the steepest slopes of the basin.

[6] The geometry of the active submarine fault system at the seabed was determined from analysis of high-resolution multibeam bathymetric data collected in the north Marmara trough (fault map from *Armijo et al.* [2002] reproduced in Figure 2). Present-day tectonic activity of the Çınarcık Basin seems governed by transtension between two strike-slip segments: the İzmit fault in the east (fi), which enters through the Gulf of İzmit, and the linear strike-slip transfer fault connecting the Çınarcık Basin to the Central Basin in the west (fnw). At the eastern tip of the Çınarcık Basin, 35 km SSE of Istanbul, a fresh scarp most likely corresponding to the 1999 İzmit earthquake break was located using microbathymetric data collected by a remotely operated vehicle (ROV) [*Armijo et al.*, 2005; *Uçarkus et al.*, 2006]. This observation is consistent with the rupture length suggested by aftershock activity [*Özalaybey et al.*, 2002; *Karabulut et al.*, 2002] and deduced from synthetic aperture radar (SAR) interferometry [*Çakir et al.*, 2003]. Along fnw, which originates at a 30° bend in the northern escarpment at 28°53′E and runs toward west up to the eastern edge of the Central Basin, a 3.5-km right-lateral offset of a topographic ridge was identified in the bathymetry [*Armijo et al.*, 2002]. Presently, fi and fnw form a large underlapping, releasing step-over. Along its northeastern margin, up to the bend at 28°53′E, and along its southern margin, the basin is bounded by faults having a significant extensional component of slip, also accommodating some lateral displacement. These faults are named "fn" and "fs1," respectively (Figure 2). The northeastern Çınarcık margin is characterized by a N120°E-trending, steep escarpment, where the seafloor abruptly deepens from 100 to 1250 m depth in 5 to 7 km. At the base of this escarpment lie clear en echelon active normal fault scarps, a pattern suggestive of combined extensional and strike-slip motion. West of the bend, two fault traces can be observed over a distance of 12 km, with fn at the base of the large escarpment and fnw running 1 to 2 km farther south [*Armijo et al.*, 2002]. This geometry can be interpreted as the effect of slip partitioning, where oblique slip at depth is accommodated on two subparallel faults at the surface, having almost pure normal and strike-slip motions [*Armijo et al.*, 2002]. The southern slope of the Çınarcık Basin is more irregular and less steep than the northern one. Active faults at the seabed are a major fault striking N100°E and a series of N125°E-trending small en echelon normal faults to the southeast which extend far into the basin center [*Armijo et al.*, 2002]. Again, the en echelon pattern suggests that this area is the site of combined

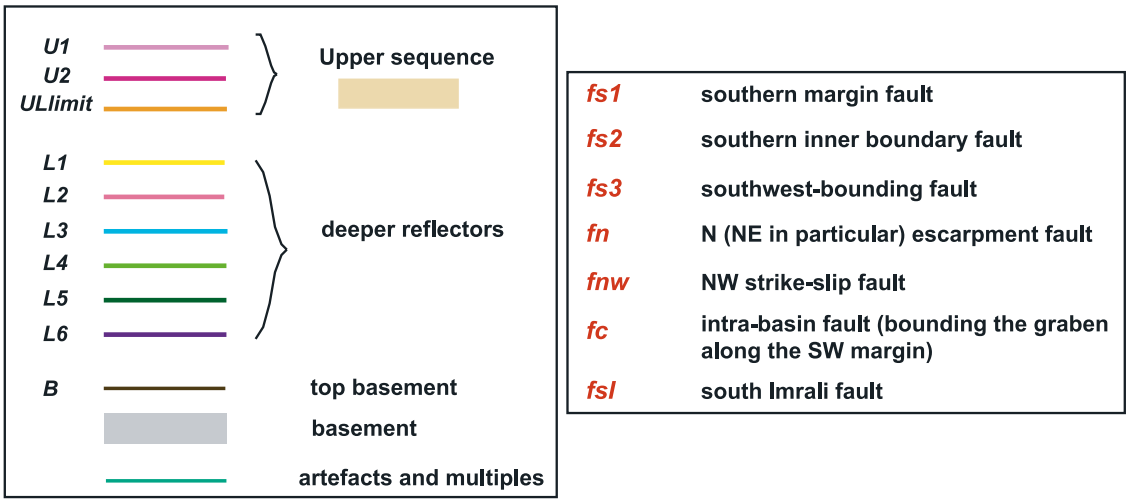

Figure 3. Horizons and faults mapped in seismic sections across the Çınarcık Basin.

extensional and strike-slip motion. West of the field of small normal faults, where the basin attains its maximum width, a deep is visible in the bathymetry along its SW margin.

[7] According to several authors [*Le Pichon et al.*, 2001; *İmren et al.*, 2001; *Rangin et al.*, 2004], extension in the deep Marmara Sea basins is dead, and the Sea of Marmara is now bypassed by a throughgoing pure strike-slip fault, the Main Marmara Fault (MMF), which established some 200,000 years ago and directly connects the İzmit fault with the Ganos fault. In the eastern Sea of Marmara, the MMF mapped by *Le Pichon et al.* [2001] follows the northern Çınarcık margin, while the field of small normal faults in the southeast of the basin is considered the only active, but very minor, extensional feature. In this model, the north-bounding fault does not accommodate any extensional component of motion, and there is no active south-bounding fault. However, the trace of the MMF as mapped by *Le Pichon et al.* [2001] encounters two major bends, at the western extremity of the strike-slip İzmit fault segment and at 28°53′N, respectively, with clear changes in strike. Hence the MMF deviates twice from the best fitting İzmit-Marmara small circle arc, representing the idealized plate boundary. This rather corresponds to a releasing double bend on a right-lateral fault, and the implications of this increased geometrical complexity are the following: either the MMF is locally not a pure strike-slip fault but is transtensional along the NE Çınarcık margin or there are other unmapped active faults on the southern margin that accommodate the extension inside the double bend. In a nutshell, extension needs to be taken up by the border fault on the northern side of the Çınarcık Basin and/or by one or several other faults on the southern margin.

2.2. Seismicity

[8] Current microseismicity records, especially aftershocks of the 1999 İzmit earthquake, indicate mixed focal mechanisms: strike-slip, extensional, and oblique-slip mechanisms are observed in the Çınarcık Basin [*Özalaybey et al.*, 2002; *Karabulut et al.*, 2002; *Sato et al.*, 2004]. Besides, Istanbul and surrounding areas were repeatedly hit by damaging earthquakes in the historical period [e.g., *Ambraseys and Finkel*, 1991]. The 1719 event, the first of the famous eighteenth-century earthquake sequence, is thought to have broken the İzmit fault. Earthquakes which may have occurred on the Çınarcık Basin margin faults include the 1754 event (maybe rupturing the NE segment) and the 1894 event (rupturing the south or NE segment) [e.g., *Parsons*, 2004]. More recently, the 1963 Mw = 6.3 earthquake is thought to have broken part of the NE Çınarcık Basin fault with an epicentral location of 29°12′E, 40°54′N [*Taymaz et al.*, 1991]. *Armijo et al.* [2005] observed a small fresh break 20–30 km long along the NE Çınarcık Basin fault, which might correspond to the 1963 earthquake rupture. Coulomb stress modeling [*Pondard et al.*, 2007] shows that the scenario that best accounts for the eighteenth-century earthquake sequence is the following: 1719 on the İzmit fault, 1754 on the NE Çınarcık fault, May 1766 on the central strike-slip segment (fnw), August 1766 on the western strike-slip segment, and Ganos fault, thus following a westward migration scheme. To the east, twentieth-century earthquakes include the 1999 event on the İzmit fault and the 1963 event as discussed earlier. To the west, the 1912 Ganos earthquake rupture may extend under water up to the SW corner of the Central Basin [*Armijo et al.*, 2005]. The central strike-slip segment that connects the Çınarcık and Central basins (fnw) probably last ruptured in 1766 and therefore constitutes an imminent threat to the city of Istanbul and neighboring areas [*Pondard et al.*, 2007]. It is the same segment which might have ruptured in 1509, producing an extremely destructive earthquake [e.g., *Ambraseys and Jackson*, 2000]. There is also evidence for historical tsunamis in the Sea of Marmara, especially in the vicinity of Istanbul. Results from numerical modeling, where tsunami sources are either coseismic displacements or landsliding, show that a significant normal component on the northern margin of the Çınarcık Basin is required to explain the waves observed in Istanbul [*Hébert et al.*, 2005].

3. Data Analysis

[9] Seismic data of the SEISMARMARA experiment were collected aboard the French research vessel "Le Nadir" using a 2860-cu.in. air gun array tuned in single-bubble

mode [e.g., *Avedik et al.*, 1993] and a 4.5-km long digital streamer. In the Çınarcık Basin area, 82 dip lines with N13°E azimuth and one strike line were shot at 37.5-m intervals, totaling over 2000 km of profiles (Figure 2). Air guns were towed at different depths (between 18 and 28 m), in order to enhance the bubbles at the optimum tow depth for each gun. The single-bubble source configuration aims at aligning the first bubble-pulses rather than the primary pressure spikes in the conventional manner, which leads for the same volume to a greater penetration because of the low-frequency content of the bubble pulse. It provided a low-frequency, energetic but ringy source signature which was used for simultaneous streamer and OBS recording.

[10] Processing of the SEISMARMARA data was carried out using Focus software. Seismic reflection data were resampled from 4 to 8 ms and sorted into common midpoint (CMP) gathers (60-fold coverage) at 6.25-m spacing along ship track. A multiple-suppression technique using the parabolic Radon transform was applied to suppress the water bottom multiples. This required, for any specified CMP location, a user-defined velocity law intermediate between the velocity of the primaries and the velocity of the multiples. After normal moveout correction with this velocity law, unwanted multiples, which had positive moveout, were forward transformed and subtracted from the initial data. Velocity analysis was carried out by semblance analysis on supergathers at every 100 to 300 CMPs. The stacked sections were subsequently time-migrated with Kirchhoff algorithm using a velocity model derived from stacking velocity picks. Trace mixing (with a 1-3-1 mix) and an automatic gain control (with an 800-ms window length) were used for display purposes. No depth sections were produced, since the velocity model obtained through semblance analysis may be precise enough in the first few kilometers of sediments in the basin but not for the deep structure where moveout becomes very small. However, coincident OBS data from the same survey are under investigation using three-dimensional traveltime tomography [*Dessa et al.*, 2005], and the results will provide a velocity model suitable for depth-conversion of the time-migrated profiles. Processed seismic profiles (stacks and time-migrated sections) in SEG-Y format as well as navigation data are available for download at the following address: http://www.ipgp.jussieu.fr/~singh/DATA-SEISMARMARA/.

[11] Following these processing steps, interpretation of the time-migrated profiles was carried out using a line-based interpretation package (SeisX), which only requires importation of two-dimensional profiles in SEG-Y format and corresponding navigation data and allows picking of horizons and faults with a good control at crossover points. Higher-resolution data from the 1997 survey conducted onboard R/V Sismik 1 from General Directorate of Mineral Research and Exploration (MTA), processed (including 1500 m/s time migration) by *Parke et al.* [2003], were included to form an eastern Marmara Sea grid. These data provide complementary information regarding the fine-scale, shallow structure of the basin and surrounding areas. Therefore whenever a horizon was identified on both data sets, it was picked first on the MTA data and then on the SEISMARMARA data to ensure that the picked phase was correct. Thickness maps were produced for all the reflectors interpreted in the seismic sections as the difference (in ms two-way time) between horizon picks along the seismic profiles and the seafloor time.

4. Results and Interpretations

4.1. Mapped Horizons and Faults

[12] The names of horizons and faults we shall refer to and discuss in the following are shown in Figure 3. The fault nomenclature is as follows: "f" stands for fault, "n" stands for north, "s" stands for south, and "c" stands for central.

[13] A very important horizon to identify is the boundary between Pliocene-Quaternary syntransform sediments, deposited after propagation of the NAF in the Marmara region [*Armijo et al.*, 1999], and the Miocene and older pretransform strata [*Okay et al.*, 2000; *Parke et al.*, 2002], deposited before the NAF was present. This syntransform/pretransform limit is thus called "basement" horizon. The contact surface between basement and basin sediments is marked here as a brown line, while rocks underneath are colored in grey. The variety of outcropping rocks on the Marmara Sea shores, including pre-Miocene volcanic, sedimentary, and metamorphic rocks, suggests a heterogeneous basement. Upper Cretaceous (UC) limestones form part of the acoustic basement beneath the southern Marmara Sea basins such as the İmrali Basin [*Parke et al.*, 2002]. These rocks crop out on İmrali Island and have been found at 2174 m depth, overlain unconformably by Upper Miocene-Pliocene calcareous mudstones and sandstones, in the MARMARA 1 well on the southern shelf [*Ergün and Özel*, 1995]. The unconformity between high-velocity UC limestones and overlying sediments generates a strong impedance contrast [*Parke et al.*, 2002], thus probably accounting for the high-amplitude reflector observed on the southern edge of all the SEISMARMARA profiles. The pretransform rocks in the Çınarcık Basin area may also include sediments from the Tertiary Thrace Basin [*Ergün and Özel*, 1995].

[14] Several reflectors, marked as colored horizons, were identified within the synkinematic sediments on part or all of the seismic profiles crossing the Çınarcık Basin. In particular, a very clear, relatively shallow reflector was mapped in most of the profiles, defining the base of what *Okay et al.* [2000] and *Parke et al.* [1999, 2002] called the "Upper sequence", in opposition with underlying (more deformed) sediments and disturbed slope deposits. This reflector ("ULlimit") is indicated with an orange color on the profiles, and the sediments above are colored in light orange. These shallow sediments have low P-wave velocity, 1.5 to 1.7 km/s interval velocity inferred from velocity analyses, and their thickness varies from 0 to 950 ms twt, globally increasing eastward. Two intermediate reflectors were mapped within the Upper sequence, and were called U1 and U2, where "U" stands for "Upper sequence". Sediments below reflector ULlimit have higher P-wave velocities, increasing downward from 1.7 to about 3.8 km/s; mapped horizons were called "L1" to "L6," where "L" stands for "Lower sequence" (Figure 3). In addition, a green-blue color was used to indicate remaining multiples, which are especially visible in areas where the seafloor topography changes very rapidly, and artifacts like side-swipes that conspicuously cut across horizons imaged by subvertical rays.

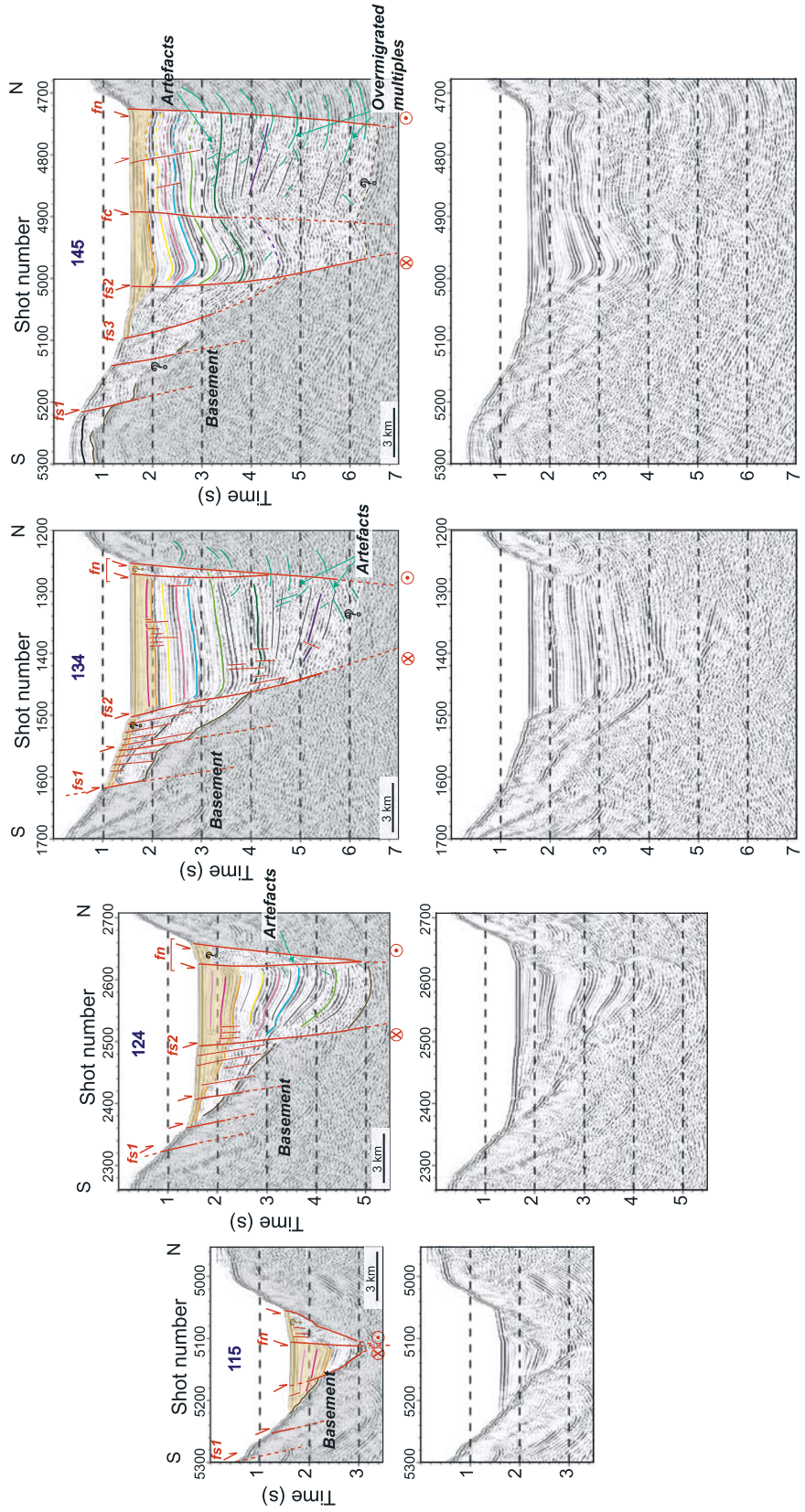

Figure 4. Selected north-south profiles (115, 124, 134, and 145) from the eastern half of the Çınarcık Basin grid. Bottom plots: two-dimensional time-migrated sections; top plots: interpreted sections. Profiles are displayed with a vertical exaggeration of 4 at the seafloor, which corresponds to a vertical exaggeration of 3 within sedimentary layers having 2 km/s velocity. See text for discussion.

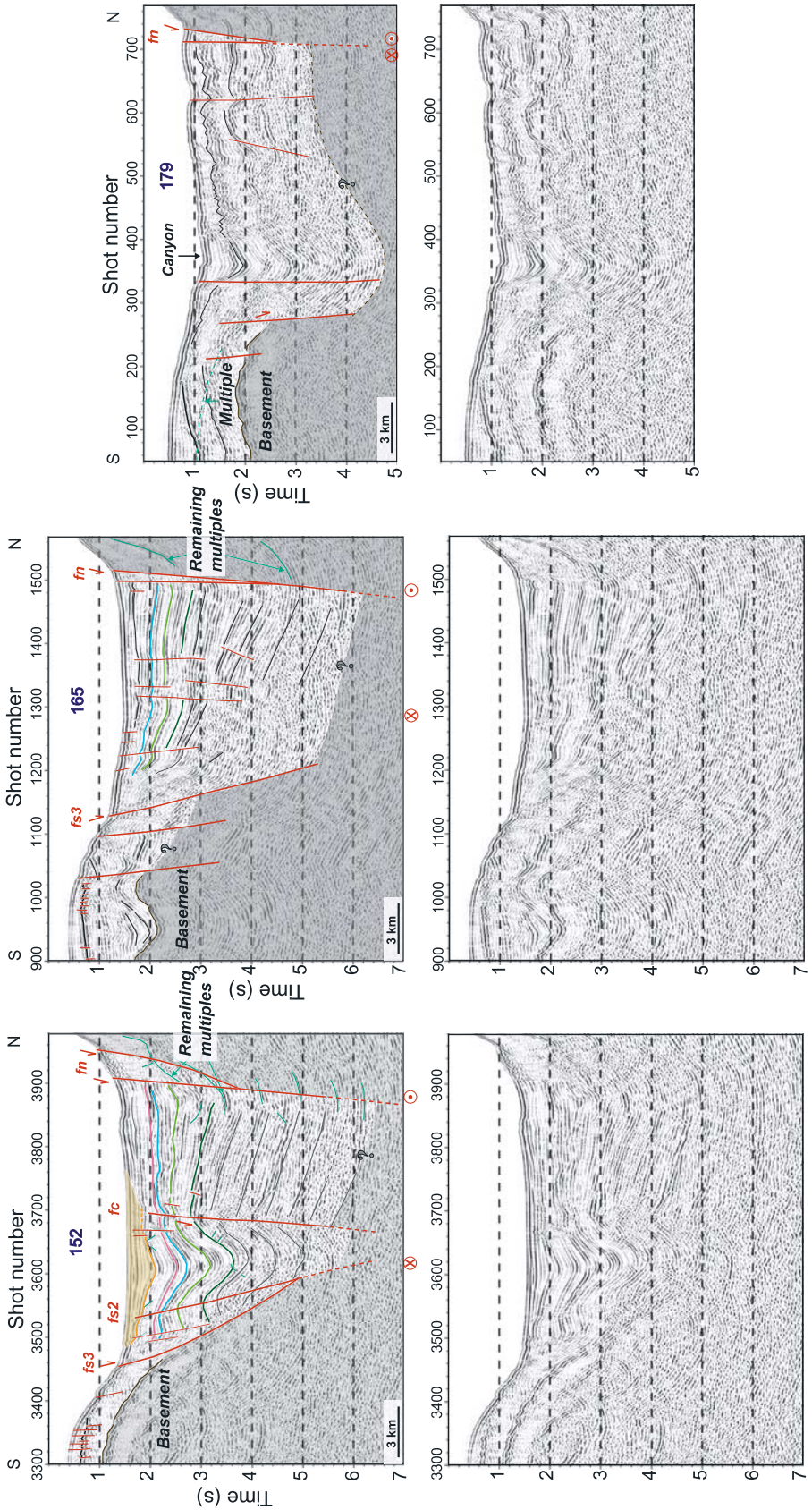

Figure 5. Selected north-south profiles (152, 165, and 179) from the western half of the Çınarcık Basin grid. Bottom plots: two-dimensional time-migrated sections; top plots: interpreted sections. See text for discussion.

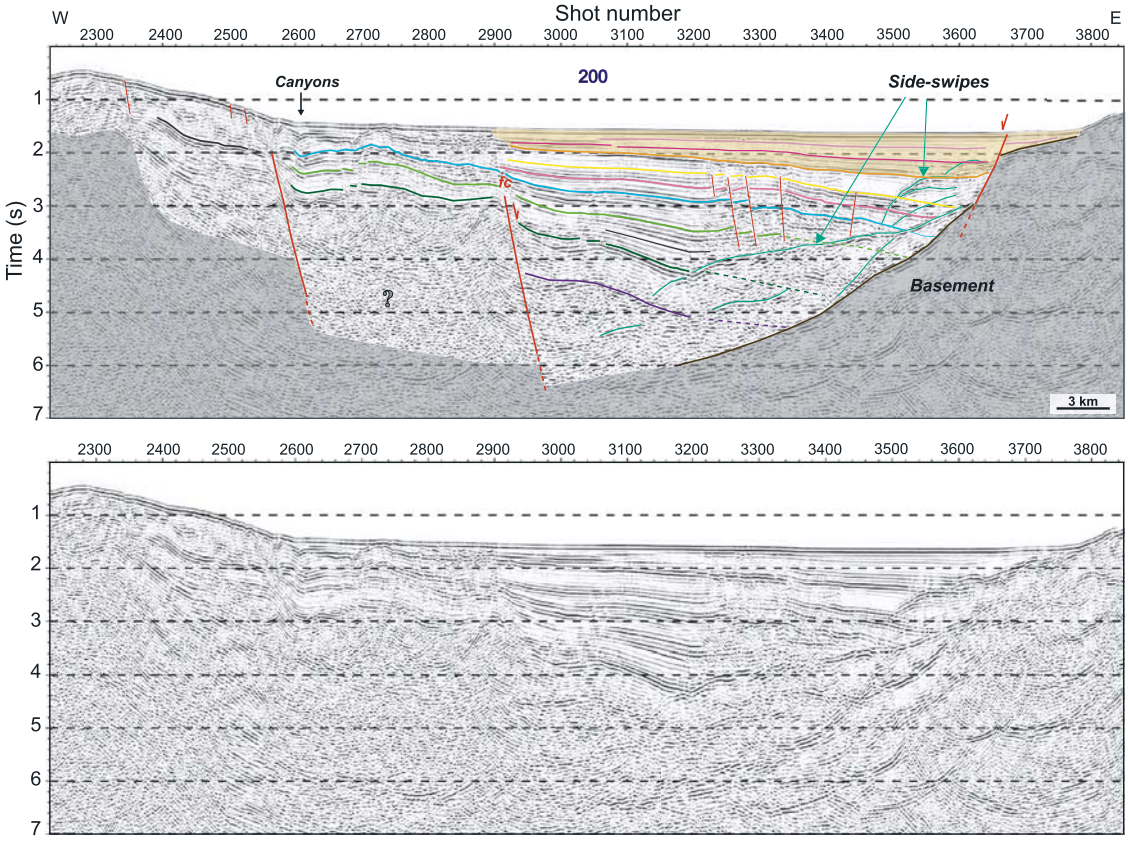

Figure 6. Strike line (200), two-dimensional time-migrated, and interpreted sections. See text for discussion.

[15] The absence of wells in the Çınarcık Basin implies that reflectors identified in seismic sections are neither constrained in terms of lithologic contrasts nor in terms of age. Analysis of the long cores collected during the MARMACORE cruise in 2001 showed that the central pull-apart of the Central Basin [*Armijo et al.*, 2005] as well as the deepest areas of the Çınarcık Basin (R. Armijo, personal communication, 2005) have sedimentation rates of 3 mm/yr for the Holocene, whereas the outer part of the Central Basin has a sedimentation rate of 1 mm/yr for the Holocene. This is consistent with the fact that fault-bounded bathymetric deeps are typically the site of the highest sedimentation rates. By contrast, sedimentation rates are much smaller on the shallow platform areas (less than 200 m water depth), between 0.13 and 0.52 mm/yr [*Çatagay et al.*, 2000].

[16] Fault mapping was carried out as follows. A few major faults were mapped first, then smaller features were progressively added wherever supported by the data. There was generally an excellent correlation with high-resolution bathymetry as well as 3.5 kHz mud-penetrator profiles (G. Uçarkus, personal communication, 2006): faults that were easily identified in the near-surface data and showed vertical throws were systematically present through inflections at the seabed in the multichannel seismic sections, and their continuations at depth were revealed. In addition, several faults which had little or no expression in the seafloor morphology could be mapped from the seismic profiles (Figure 2). The least detectable feature of all in the seismics was the strike-slip branch fnw, an observation that is hardly surprising since seismic profiles essentially allow to recognize a fault through its dip-slip component. The location of fnw was marked onto the seismic images on the basis of the sharp trace visible in the bathymetric data. Neighboring sediments were disturbed in the seismic sections, but there was generally no clear indication about where to mark the fault. To some extent, fs1 was also difficult to identify, except where a significant offset in the basement was present. Another issue for interpretation is that the SEISMARMARA data are very low frequency with a long source wavelet (400 ms), which results in a poor vertical resolution: it is difficult to distinguish between two horizons having a vertical separation less than 200–300 m. Even though the lateral sampling is very good (1 CMP trace every 6.25 m), there is an overall lack of sharpness of the images. However, the limited vertical resolution of the seismic data did not prevent the observation of vertical offsets of about 40 m at the seabed (the aforementioned inflections). Indeed, what is considered here is a single horizon whose lateral sampling is very good and which is overlain by a transparent layer (water). The dense grid of profiles were highly valuable material to establish correlations from one profile to another and thus to assess the along-strike continuity. They also helped distinguish between artifacts (side-swipes, multiples) and real features. The smaller faults were found to be scarcely continuous over more than two consecutive profiles, while the major faults were as carefully mapped as possible throughout the grid of lines. The lines presented in this paper

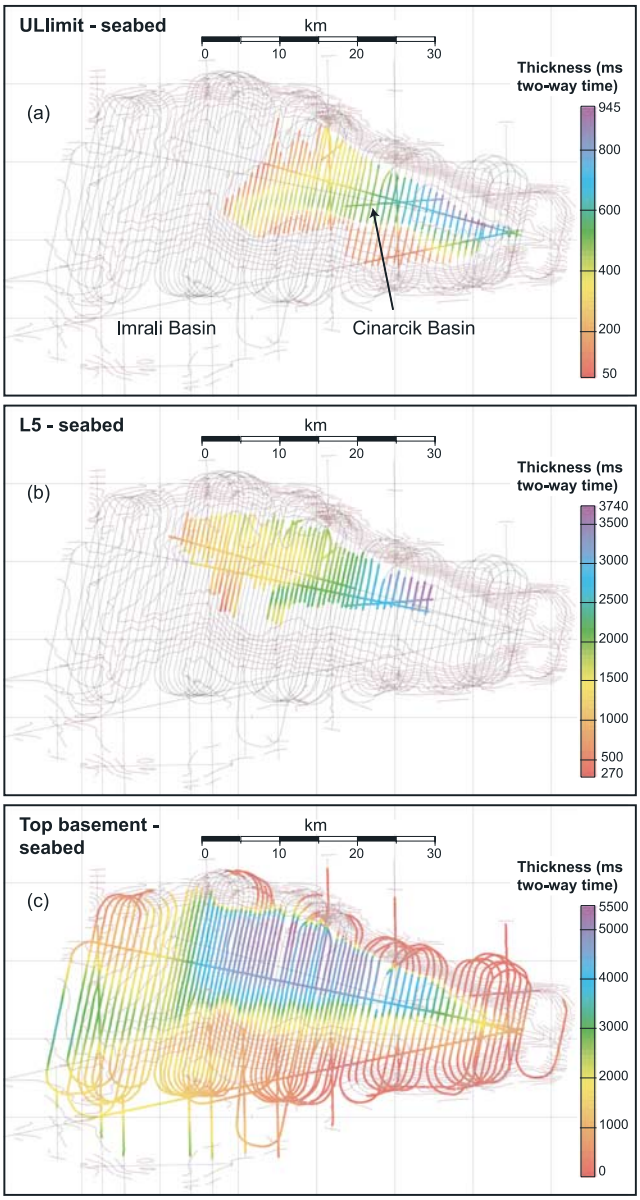

Figure 7. Thickness maps in ms two-way time for the Çınarcık Basin area, constructed as the difference between horizon picks along seismic profiles and seafloor time. (a) ULlimit-seabed, (b) L5-seabed, (c) top basement-seabed. Layer thicknesses are superimposed onto smooth bathymetric contours interpolated from seafloor picks on the seismic profiles. Most of the survey area was covered by the SEISMARMARA data, which are characterized by a long source wavelet. Therefore thickness values $\leq$150 ms on the global maps are not significant (i.e., equivalent to 0) because any reflector within this time window cannot be distinguished from the seafloor reflection.

were selected because they showed the clearest features as well as minimum artifacts.

4.2. Interpreted Profiles

[17] Several interpreted profiles are presented here as two-dimensional lines, from west to east (Figures 4, 5, and 6), and will be described in the following paragraphs. All the seismic sections are displayed with a vertical exaggeration of 4 at the seafloor, which corresponds to a vertical exaggeration of 3 within sedimentary layers having 2 km/s velocity.

[18] Profile 115 crosses the basin 11–12 km west of the termination of the İzmit earthquake break, as observed by *Armijo et al.* [2005] and *Uçarkus et al.* [2006] (Figure 2). The sediment deposition is asymmetric, contrasting with flat-lying horizons farther east, where the basin narrows toward the Gulf of İzmit. Here the basin is bounded to the north by two faults: a very steep innermost fault, associated with a clear normal scarp at the seafloor, and an outer branch lying at the base of the main escarpment. In between these two fault branches lie disturbed sediments, whose internal structure is not resolved by the data, possibly including some Upper sequence sediments. To the south, the rest of the basin fill shows regularly bedded, north-dipping sediments, among which horizons U1 (light purple), U2 (purple), and ULlimit (orange) are identified. The basement reflector seems to be displaced by a major fault, with a vertical throw of 950 ms. Fault fs1 is crossed at the southern end of the profile. The fact that sediments dip to the north in most of the basin suggests that in this part of the basin, vertical motion on the northern side has been greater than vertical motion on the southern side.

[19] Profile 124 is situated south of Prince's Islands, 7.5 km west of profile 115. The basin is bounded on the northern side by two steep branches that appear to connect at depth into a single fault fn. Toward the middle of the line, a basement block is offset by fault "fs2", which appears to be a major boundary. This fault, also observed on most profiles farther west, corresponds to the "Inner Boundary Fault" identified by *Okay et al.* [2000]. In the southern half of the basin, numerous small normal faults cut through shallow sediments with generally little vertical displacement. These small faults, which according to high-resolution bathymetric data display an en echelon pattern (Figure 2), are also well imaged using high-resolution 3.5 kHz mud-penetrator profiles (G. Uçarkus, personal communication, 2006). On the southern margin, inflections in the seafloor topography are interpreted as indicating the presence of faults, although the extension at depth of these basement faults cannot be imaged. The main fault fs1, a second fault at the tip of the sediment wedge, and a third fault responsible for an offset in the basement are imaged. The bottom of the basin is encountered at more than 5 s two-way time near the innermost branch of fn. Horizons L1 (yellow), L2 (pink), L3 (blue), and L4 (spring green) are identified. Moreover, this profile shows a very clear ULlimit horizon over most of the basin width. By contrast, in the part of the basin south of fs2, it is impossible to identify reflectors deeper than ULlimit (continuations of L1, L2, L3, or L4 in the footwall of fs2).

[20] Profile 134, which runs 8.5 km west of profile 124, confirms that fault fs2 is a major boundary between the deep basin and marginal areas with offset basement blocks, hence its name of Inner Boundary Fault. South of fs2 extends the field of normal faults. This profile also highlights the importance of fault fs1, which is the southern margin fault mapped in bathymetric data by *Armijo et al.* [2002]: fs1 shows here a clear vertical offset of the basement/basin sediments contact. A deep horizon called L6 (dark purple)

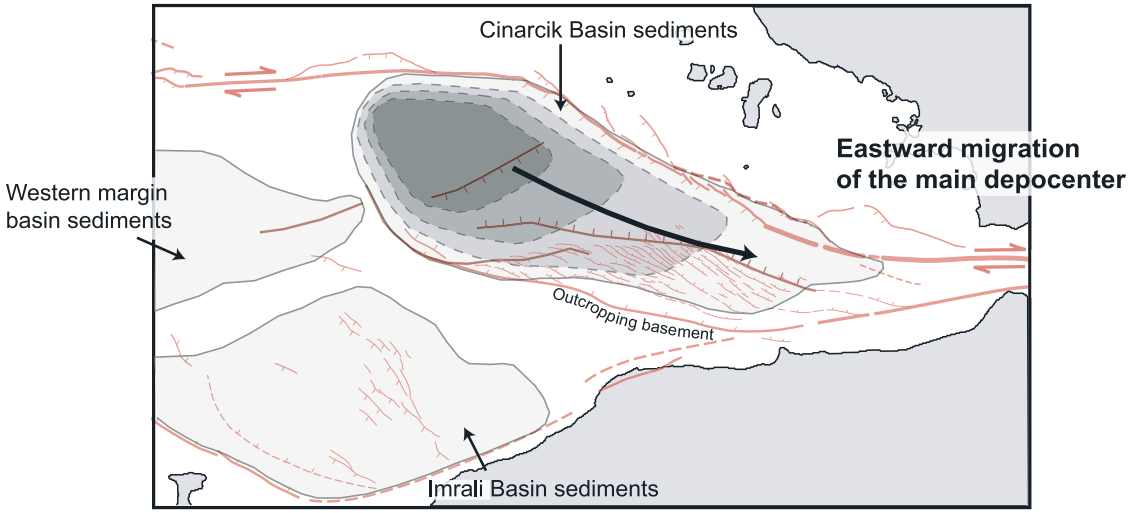

Figure 8. Map showing the location of the depocenters of the eastern Sea of Marmara and the eastward migration over time of the main depocenter of the Çınarcık Basin.

and dipping to the north is identified on this profile. The first 2.5 s of sediments are tilted toward the south, whereas deep sediments (about 2 s thick) dip toward the north. The location of the bottom of the basin is fairly speculative because of the absence of clear reflectors for times more than 6 s. Deep sediments around horizons L4 and L5 may be affected by small normal faults. The Upper sequence is thinner than on profile 124, suggesting that the Upper sequence globally thins toward the west.

[21] Profile 145, which runs 6.8 km west of profile 134, images a wider basin and a more complex structure than profile 134. It displays a new tectonic feature, a south-dipping fault called "fc" located in the center of the basin and which comes close to the surface at SP 4890. This fault forms the limit of a subbasin along the southern margin. It clearly offsets horizon L3 (blue), but its deep throw, at the base of the basin, is difficult to assess. North of fc, deep sediments are tilted toward the north, while layers above horizon L5 are more flat-lying. Reflectors imaged on the northern side of fs2 now seem almost continuous across the fault. On this profile as well as on several profiles farther west, fault fs2 appears more as a flexure than a fault, since the beds seem more distorted than offset by the fault. This might result from slow vertical motion along this fault compared to sedimentation rates. Moreover, all the profiles here are displayed with a vertical exaggeration of 4 at the seafloor, which is equivalent to a vertical exaggeration of 3 at 2 km/s (a good approximation for the first 2–3 km of sediments), hence true dips are considerably reduced compared to apparent dips on the time sections plotted here.

[22] Profile 152, located 4.2 km farther west, crosses the north-bounding fault fn almost at right angle, west of the bend at 28°53′N. The basin is wider, and the subbasin along the southern margin is now fully developed. This feature looks very peculiar in the seismics because of its more or less symmetrical syncline shape. Fault fc forms the boundary between sinking sediments in the south and north-dipping sediments in the north. Fault fn consists of two branches, an inner, steep branch along which basin sediments terminate and an outer branch located at the base of the main slope. The basement reflector on the southern side appears as a round-shaped high-amplitude reflector, overlain by ~700 ms of sediments.

[23] Profile 165, located 7.8 km west of profile 152, displays a simpler image: the subbasin has disappeared, and the southern side of the Çınarcık Basin is characterized by normal faulting on "fs3" and possibly on two other faults south of fs3. The basement reflector is visible at the southern end of the profile. Above it, between SP 900–1100, there is another strong reflector which shows a complex topography and may be faulted. On the northern side, well-stratified basin sediments are tilted toward the north, terminating against a fault which seems to split into two close branches. It is unclear where the bottom of the basin lies here, but it might be dipping toward the north.

[24] Profile 179 runs across the western flank of the Çınarcık Basin, 9.4 km west of profile 165. The basement is clearly imaged in the south. Between SP 400–700, disturbed sediments are imaged, which have possibly undergone some compression. A canyon is crossed, and the deeper structure shows V-shaped reflectors. To the south, the canyon seems bounded by a fault at SP 330; there are two other faults on the southern margin associated with basement offsets at SP 270 and SP 210. Sedimentary thickness may reach 3.7 s near the fault at SP 330 and decrease toward the north. The northern escarpment is crossed at SP 710–730. This profile suggests that the western flank of the Çınarcık Basin is occupied by another basin and that a major fault exists that bounds the canyon to the south. This basin is seen to continue on the lines 180–188 shot farther west toward Central High.

[25] Profile 200, which is 57 km in length, was shot at right angle to the cross-lines, i.e., with an azimuth of N10°E (Figure 2). It provided very useful information to connect all the other profiles and was extensively used during the horizon-picking phase. However, this profile remains difficult to interpret since it comes close to the northern escarpment in its eastern part, hence the presence of side-swipes events, and also because the major faults are not imaged. In the eastern half of line 200, eastward-thickening

sedimentary layers terminate against the west-dipping basement reflector. Interestingly, fault fc (imaged on lines 145 to 156) is also crossed here, and although this fault does not reach the surface, it marks a clear boundary between the eastern and western halves of the basin. At the eastern end of the profile, a fault coming to the surface is imaged, probably a SW-dipping fault segment at the entrance of the basin. East of fc, sediments are dipping toward the east, with some local complexities related to the field of normal faults that extends far into the basin. Horizons seem to terminate against a high-amplitude reflector, which we interpret as the top of the basement. The eastern part of the profile also displays curved, sometimes quite continuous events which seem uncorrelated with mapped horizons. These are most probably out-of the plane events, corresponding to reflections or diffractions on the steep basin sidewalls. Horizons L1, L2, L3 and to some extent deeper reflectors are seen cutting across these events. West of fc, the picture becomes more complicated, and correlation of horizons on the eastern and western sides of the fault is difficult. Basin floor shallows west of SP 2560, suggesting at this location the presence of a deep fault defining the western boundary of the basin.

4.3. Thickness Maps

[26] Mapping variations in sedimentary thicknesses from the seismic reflection data grid is the key to understanding the formation of the basin and the role of the different faults. The lateral continuity of events was generally good in the eastern part of the Çınarcık Basin, although it was hardly ever possible to extend horizon picks on the edges of the basin, on either side of the innermost bounding faults (see for instance profiles 124 and 134 on Figure 4). As already seen on profile 200 (Figure 6), correlation of horizons within the basin on the northwestern and southeastern sides of fault fc remained speculative. In the western half, difficulties came from the presence of remaining multiple energy at depth which made it harder to identify and follow true reflectors (including L6 and the basement reflector). Also, profiles running on the western flank of the Çınarcık Basin toward Central High (profile numbers 170–188 approximately) are characterized by a poor imaging quality, which suggests they sample a deformed area.

[27] Upper sequence sediments (Figure 7a) are seen in the flat, deep part of the Çınarcık Basin and thicken eastward. The maximum thickness is found in the eastern part of the basin along the north-bounding fault: ~950 ms twt (e.g., line 117), which corresponds to a thickness of 760 m at a velocity of 1.6 km/s. As the basin floor shallows westward, a regular thinning of the Upper sequence is observed, with a local thickening in the SW part of the basin inside the subbasin imaged on line 152. Correlation between layer thicknesses and bathymetry is obvious for this reflector, i.e., thick Upper sequence sediments are observed where the seafloor is deep. The second plot (Figure 7b) shows the cumulated thickness down to horizon L5, and westward thinning is also observed.

[28] A total sedimentary thickness map (Figure 7c) was produced in and around the Çınarcık Basin using a smooth interpretation of the basement. The basement reflector is well-defined in the İmrali Basin and in the eastern half of the Çınarcık Basin, where the total sedimentary fill is less than 3–4 km thick. Farther west in the Çınarcık Basin, deep sediments are imaged, but the bottom of the basin can be mapped with limited confidence using our reflection profiles. There is no real clear, high-amplitude reflector, and in some places remaining multiple energy is a severe problem, with overmigrated seafloor multiples obscuring deep reflections. The maximum sedimentary thickness in the Çınarcık Basin is about 5–5.5 s twt (5–6 km using an average velocity of 2–2.5 km/s) along the north-bounding fault, south and southwest of the bend in the northern escarpment; therefore the bottom of the basin may seem downthrown to the north. Total sedimentary thickness values equal to 0 on the SE side of the Çınarcık Basin (red color) correspond to an area where Upper Cretaceous limestones are exhumed on the southern slope of the Çınarcık Basin, whereas they are covered by sediments farther west. In the westernmost 15 km of the survey area, another basin is imaged (e.g., line 179), which seems to continue westward toward the Central High. Sediment thickness in this basin is difficult to map precisely because of the difficulty to identify the basement reflector, but their total thickness may be ~3–4 s. This basin seems bounded to the south by an ENE-WSW trending fault. In the İmrali Basin, sediments are observed to thicken southward.

[29] In summary, the widest part of the Çınarcık Basin, south and southwest of the bend in the northern escarpment, seems to be the site of accumulation of the thickest sediments and thus probably the oldest part of the basin (Figure 8); in this area, a smaller subbasin is also imaged along the southern margin. There seems to exist another basin located on the western margin of the Çınarcık Basin toward Central High, filled by sediments up to 3–4 s thick and bounded to the south by a NNE-SSW trending fault. The area which has undergone the maximum amount of extension in recent times (a few 100,000 years) is the eastern part of the basin, as indicated by the Upper sequence thickness map. This area coincides with the area of maximum seafloor depth in the basin, which is consistent with greater vertical displacement, especially along the north-bounding fault. The distribution of sediments described here suggests an eastward migration over time of the main depocenter of the Çınarcık Basin (Figure 8).

5. Discussion: Tectonic Evolution of the Çınarcık Basin

5.1. Three-Dimensional Views

[30] Evolution of the structure of the basin on its northern side is highlighted in Figure 9. The basin is bounded by a large and steep northern fault fn. Two branches are often observed, one inner branch carrying more strike-slip displacement and one outer branch carrying more extensional displacement, both probably merging at depth into a same transtensional fault. Thick sediments, probably up to 6 km thick (e.g., profiles 145 and 165), are imaged along this fault. More specifically, easternmost profiles 122, 128, 136, as well as the strike line 200 show a westward deepening of the bottom of the basin which coincides with more horizons being mapped in the seismic sections. Farther west, it is delicate to identify the bottom of the basin, but still several seconds of sediments are imaged everywhere. Northward tilting of deep sediments is visible throughout most of the

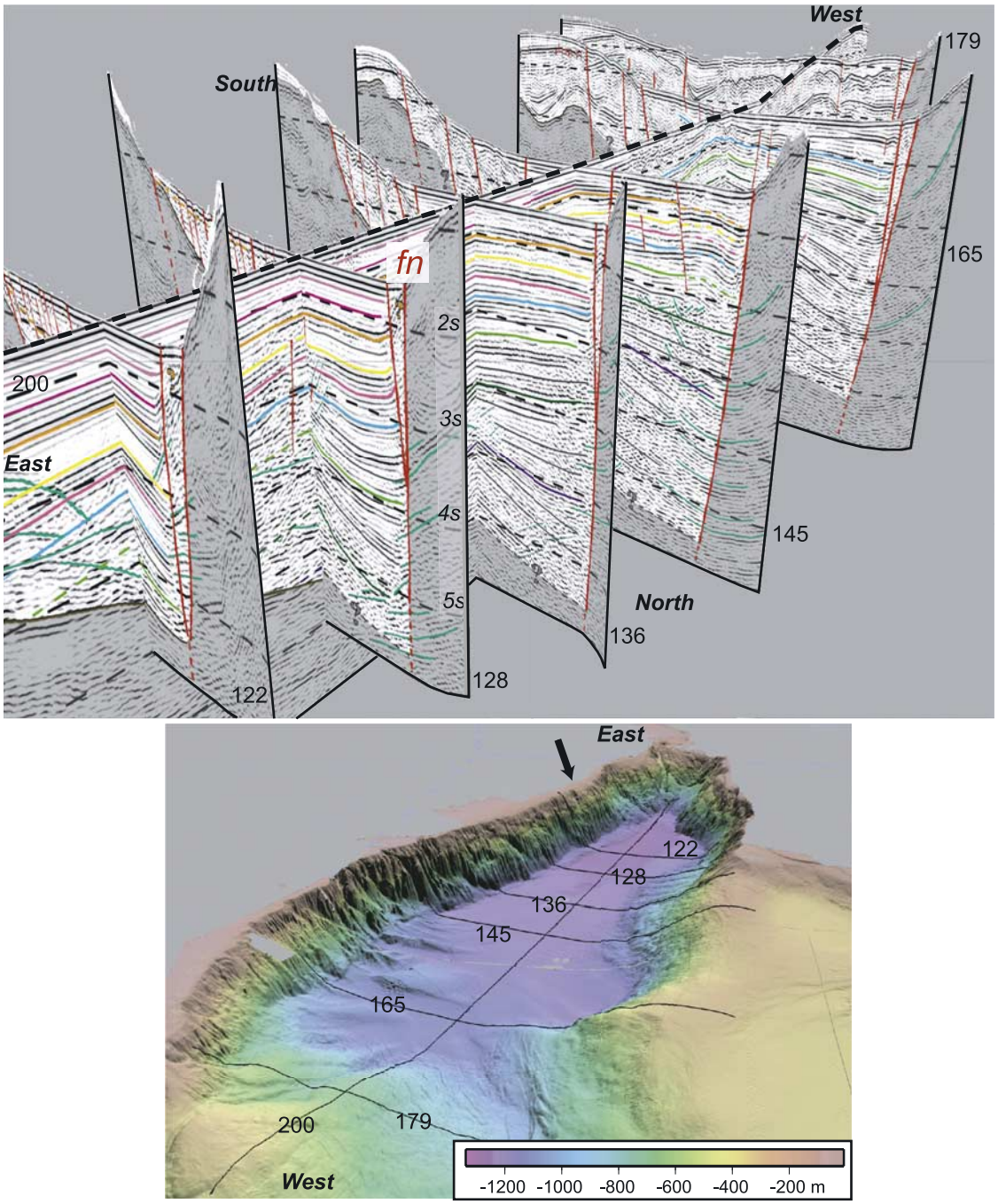

Figure 9. Top: three-dimensional view of selected seismic profiles from the northeast and thus emphasizing the north side of the Çınarcık Basin (east is on the left handside, west is on the right handside). Bottom: three-dimensional high-resolution bathymetry of the whole Çınarcık Basin with location of seismic lines draped onto the seafloor; view is from the southwest instead of northeast, since if the same azimuth/elevation had been chosen as for the seismics plots, the basin would have been hidden behind the northern escarpment. Interpreted profiles suggest long-term activity on the northern escarpment.

basin up to at least profile 165 in the west. Shallower sediments show a more varying pattern. On profile 122, fanning toward the northern margin is observed on the whole section. By contrast, on profile 128, sedimentary layers above horizon L4 are roughly symmetrical and almost flat-lying, suggesting that at this location, dip-slip motion on the north-bounding faults must have been dominant in a first phase of opening of the basin; a second phase followed, during which faults on both sides have taken the same amount of vertical displacement. On profile 136,

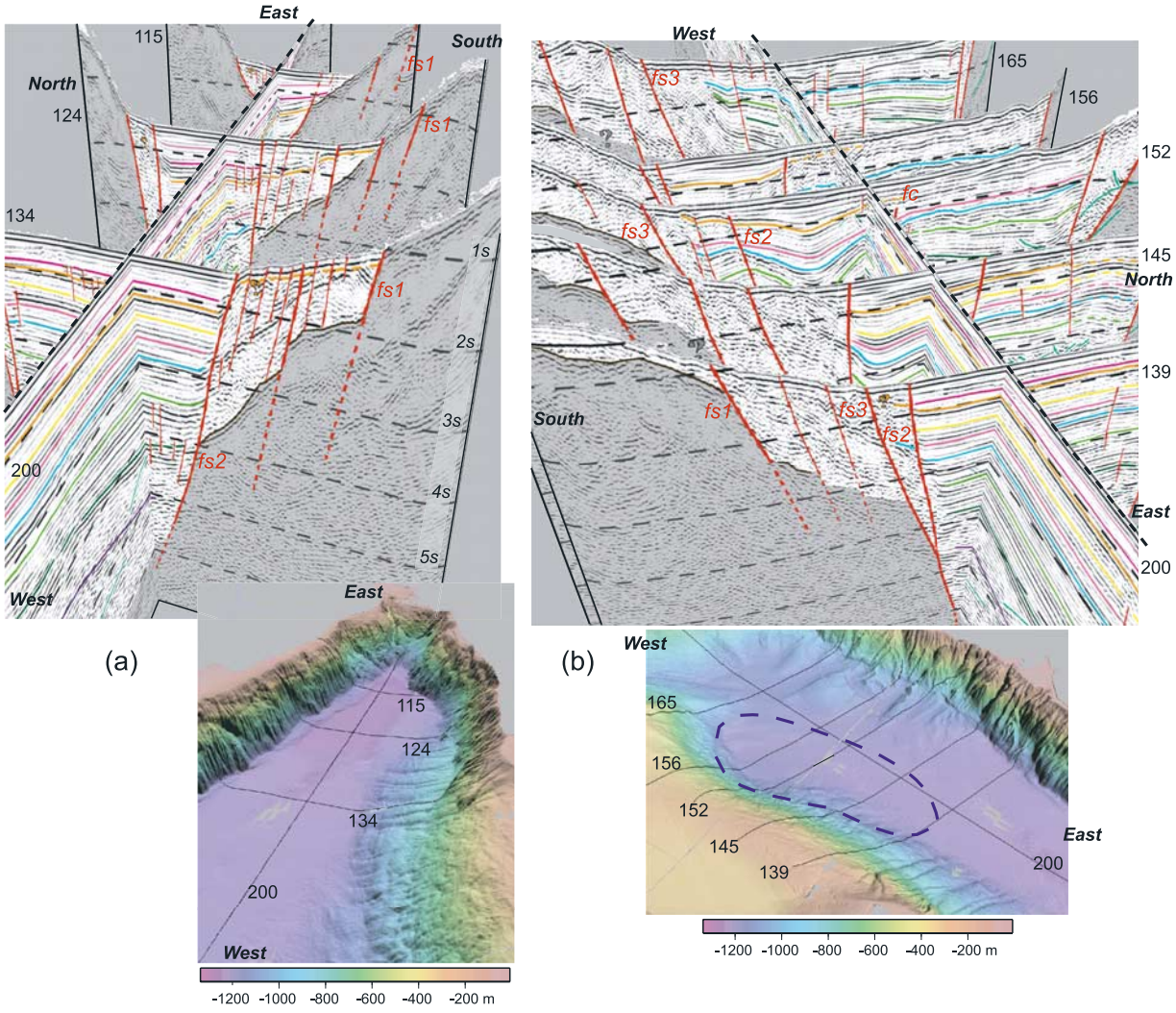

Figure 10. Three-dimensional views emphasizing the south side of the Çınarcık Basin. (a) View from the west showing the eastern half of the basin, with location of the profiles displayed onto the bathymetric surface (same azimuth but zoomed out) (b) View from the southeast showing the subsurface expression of the subbasin, with location of the profiles displayed onto the bathymetric surface (slightly different azimuth and zoomed out). Blue dotted line shows the approximate contours of the subbasin.

motion on the south-bounding faults must have dominated in the recent phase since sedimentary layers above horizon L4 dip toward the south. In a nutshell, the data provide evidence of steady activity including dip-slip motion along fn since the beginning of opening of the basin. This is in agreement with the very steep slope along the entire north Çınarcık escarpment. East of the bend at 28°53′E, the inner fault produces a very clear step (50 m high) in the seafloor topography (e.g., profiles 122 and 128), whereas the outer fault is in the continuation of the main slope (1 km high escarpment). West of the bend, the NW segment presently accommodates strike-slip motion, with some slip partitioning, as imaged on profiles 165 and 179. As suggested by *Okay et al.* [2000] and *Rangin et al.* [2004], the formation of the Çınarcık Basin might have been guided by preexisting structures, such as N120°E-trending faults seen in the older Thrace Basin, among which the NE Çınarcık fault might have been reactivated as a transtensional fault.

[31] Figure 10a shows the evolution of the structure of the eastern half of the basin on its south side, while Figure 10b focuses on the structure of the southwestern margin, where a subbasin is imaged.

[32] Profile 134 on Figure 10a shows the presence of two major, distinct extensional faults, which are still active today: the main south-bounding fault fs1 mapped by *Armijo et al.* [2002], whose vertical displacement accounts for the main difference in elevation between the basin and its southern margin; the inner boundary fault fs2, which offsets the basement/basin sediments contact surface by 1 to 1.5 km in the east (e.g., profile 124). Other offsets in the basement can be identified in places and are associated with other, smaller faults. Outcropping basement on the south side is imaged on profile 134 and all the lines farther east. On profile 134, the measure of the offset of the basement block along this fault only yields a minimum value of the total vertical displacement because the basement crops out and

there must have been some erosion of an initial edge-shaped top-basement surface (uplifted footwall).

[33] On Figure 10b, profile 139 shows the presence of a second branch of fault fs2, called fs3. This fault is located at the base of the slope and marks the southern termination of the Upper sequence, while fault fs2 offsets the ULlimit reflector by a few tens of ms. There is a gentle tilting/sagging of reflectors toward fs2 that becomes more prominent westward. At the southern end of the profile, the basement is overlain by a thin sedimentary cover. The subbasin in the south is narrower, and deep sedimentary horizons inside it seem distorted. Maximum thickness of the Upper sequence is 400 ms in the center of the subbasin. Profiles 145, 152, and 156 image a deep extensional fault fc in the middle of the Çınarcık Basin, striking approximately N65°E and dipping to the SE. Combined activity along the southern margin faults and this intrabasin fault fc has created a large subbasin which can be seen in the seismic profiles between 28°45′E and 28°55′E. A coincident, though slightly smaller, deep is revealed by shaded bathymetry (Figure 10b). The size and orientation of this feature are similar to that of the central pull-apart nested in the Central Basin (Figure 1). It is therefore tempting to interpret this feature as a small pull-apart, which could have opened by transtension between two strike-slip segments: the inner boundary fault to the east, and a possible ENE-WSW trending strike-slip fault to the west, which will be discussed in the next paragraph.

[34] The existence of an ENE-WSW trending strike-slip segment connecting the SW corner of the Çınarcık Basin to the outer Central Basin south-bounding fault has been put forward to account for the opening of the Central Basin [*Cetin et al.*, 2003; *Bécel et al.*, 2004]. This fault would have acted as a transfer fault in an earlier stage of evolution of the Sea of Marmara and would be much less active now, with strike-slip motion presently localized some 12 km farther north along fnw. If such a fault exists, no surface expression can be seen within our data grid but a 5.9-km long E-W trending fault was mapped farther west on Central High (Figure 1). Also, the canyon crossed on line 179, whose orientation changes from N-S to ENE-WSW (Figure 2), could have been guided by this fault. The possible existence and role of an earlier strike-slip transfer fault between the Çınarcık and Central basins as well as the structure of Central High will be the focus of another paper.

5.2. Comparison With Models of Pull-Apart Basins

[35] The simplest, ''synoptic'' model of pull-apart basins involves two parallel, en echelon strike-slip fault segments. Subsequent strike-slip motion opens a hole in the step area, strike-slip segments link by two transverse, extensional branches, and a fault-bounded, box-shape basin develops. This model assumes a brittle upper crust and constant volume during strike-slip displacement. The amount of opening is equal to the distance between the basin-bounding faults, which is also the amount of displacement along the master strike-slip fault [e.g., *Garfunkel*, 1981]. Uniform subsidence of the basin is predicted.

[36] Few pull-apart basins in the field present a simple, box-shape geometry, and the term ''pull-apart basin'' is commonly used to qualify rhombic or sigmoidal areas of extension along strike-slip faults, formed because of a bend or jump in the master strike-slip fault, and where the basin-bounding faults have complex geometries and connections with the master strike-slip segments (see the pull-apart examples shown by *Aydin and Nur* [1982], *Mann et al.* [1983], and *Dooley and McClay* [1997]). Subsidence distribution is far from being uniform, and like in any extensional system, quantification of basin opening depends upon the geometry of basin-bounding faults at depth (planar or curved geometry of faults, presence or not of block rotations). A commonly observed deviation from the standard model is basin asymmetry; that is, the center of the basin is not a center of symmetry for the fault system and the distribution of subsidence areas. Such basins are often bounded on one side by a dominantly strike-slip fault (displaying a local change strike and a nonvertical fault plane) and on the other side by normal faults striking subparallel to the transform. Releasing bend geometry can account for the formation of these basins. *Ben-Avraham and Zoback* [1992] provided a different interpretation and put forward a process of transform-normal extension, where extension is due to divergence in plate motion and occurs perpendicular to the trace of the strike-slip fault.

[37] Theoretical studies [*Segall and Pollard*, 1980; *Rodgers*, 1980], numerical modeling in either two or three dimensions [*Bilham and King*, 1989; *Gölke et al.*, 1994; *Katzman et al.*, 1995], and analogue modeling [*Dooley and McClay*, 1997; *Rahe et al.*, 1998; *Basile and Brun*, 1999] help guide the interpretation of three-dimensional deformation observed in natural pull-apart basins. The shape, fault system, and sedimentary structure of a pull-apart basin depends upon the geometrical parameters associated with the step in the master strike-slip fault system: fault length, depth to the main fault in the basement, fault separation, and perhaps above all the length of overlap. Generally one single depocenter is predicted in the middle of the basin (full graben), with half-graben shapes toward the extremities [*Katzman et al.*, 1995; *Dooley and McClay*, 1997]. This, to some extent, is the case in the Çınarcık Basin: in its eastern half, normal motion on the northern fault dominates, with a typical half-graben structure, whereas in its western half, maximum activity has switched on the southern faults, with tilting of sediments toward the south and development of a subbasin.

[38] Analogue models that offer the best match with the shape of the Çınarcık Basin and the nature and orientation of its fault system are the 30° underlapping side-step model of *Dooley and McClay* [1997], which produces an elongate rhomboidal graben, and one of the 40° (possibly slightly asymmetrical) underlapping side-step models of *Rahe et al.* [1998]. The unexpected asymmetry in Dooley and McClay's experimental pull-aparts fits fairly well observations in the Çınarcık Basin, where the north-bounding fault is associated with a major escarpment and has played a dominant role in the formation of the basin. Analogue experiments also provide insight into how the model is deforming at depth, i.e., the deformation of the prekinematic layers which are poorly or not at all sampled by the SEISMARMARA seismic profiles. Vertical cross-sections across sandbox models [*Dooley and McClay*, 1997] show that the prekinematic layers are heavily faulted down to the base of the model, thus forming collapsed and/or tilted blocks of various sizes. Numerous intrabasin faults are

observed that sometimes affect the synkinematic sediments as well. The wider part of the basin displays the greatest complexity, but asymmetry is more pronounced toward the basin extremities.

[39] Interestingly, cross-basin faults (new strike-slip faults forming inside the basin, eventually causing a cessation of extension) are recurrent features in sandbox models. These faults, which develop in mature stages of evolution of experimental models, seem to play an important role in the extinction of pull-apart basins. This is in agreement with the observations of *Zhang et al.* [1989] on pull-apart basins along the Haiyuan fault in northwest China: the most common cause of pull-apart extinction appears to be the development of new strike-slip faults either along one of the basin-margin normal faults or diagonally across the basin, as a tendency for the strike-slip fault to straighten itself. However, there exist numerous basins identified as pull-apart basins and which are devoid of cross-basin faults, but these basins could be simply in their initial stages of evolution. The same interpretation may apply to the Çınarcık Basin, where evidence for a cross-basin strike-slip fault has been found neither in high-resolution bathymetric data (fault trace cutting the basin floor and linking the stepped master strike-slip branches) nor in seismic data (buried feature).

5.3. Comparison With Numerical Modeling Results

[40] *Muller and Aydin* [2005] used a numerical code to model the vertical deformation rates in the Sea of Marmara produced by several published fault systems [*Okay et al.*, 2000; *Le Pichon et al.*, 2001; *Armijo et al.*, 2002]; these deformation rates are compared with both seafloor morphology and structural deformation pattern of basement horizon. In the model, almost all the faults are assigned dips of 70°–90°: 90° for faults that were interpreted to be major strike-slip structures and 70° or 80° (dipping toward the center of the basin) for smaller transtensional basin-bounding faults. These steep dips are consistent with seismic imaging results for the Central Basin [*Hirn et al.*, 2003] as well as for the Çınarcık Basin (this study). Muller and Aydin found that an interpretation with a series of pull-apart basins along a master strike-slip fault (fault configuration of Armijo et al.) best produces the observed deformation pattern within the Sea of Marmara. The location and relative subsidence of the main basins within the north Marmara trough, the three transtensional basins and İmrali half-graben, are well matched. Conversely, results obtained with other fault configurations illustrate the simple fact that it is impossible to create a basin without basin-bounding faults bearing some extensional component of motion.

[41] Here we will focus on the distribution of subsidence computed by *Muller and Aydin* [2005] in the Çınarcık and İmrali basins using the fault system of Armijo et al., which we will compare with seismic results. To first order, the model predicts a global subsidence of the Çınarcık Basin, which is confirmed by basin depth and sedimentary structure in seismic profiles. This is a direct consequence of activity of both basin-bounding faults, fn on the northern side and fs1 on the southern side, whereas a basin fully downthrown to the north would be produced if only the northern branch was active. If another model were computed taking into account fault fs2 (Inner Boundary Fault on the southern side) as well, the subsidence pattern would even better match the observed seafloor morphology and seismic data. The site of highest subsidence is predicted within the eastern, narrow part of the basin, closer to the north-bounding fault than to the south-bounding one. This result fits very well with seafloor depth (deepest part of the basin) and recent subsidence (thickest Upper sequence). The eastern part of the Çınarcık Basin is opening at the tip of the İzmit fault, which connects to the NE-bounding fault through a clear bend. This pattern of subsidence is very similar to extension fractures forming at the tip of a strike-slip branch. In the broadest part of the basin, two smaller areas with high levels of subsidence are observed both on the north-bounding and south-bounding faults. On the south side, this is in agreement with our observation of a secondary graben opening along the SW margin of the basin. South of this depocenter, the high separating the Çınarcık and İmrali Basin is also imaged in our seismic data. Within İmrali Basin, the model predicts south-dipping sediments, which is confirmed by seismic images [*Parke et al.*, 1999; *Okay et al.*, 2000].

5.4. Age of the Çınarcık Basin? Toward a Relative Chronology of its Evolution

[42] There is a crucial need of deep borehole data in the Çınarcık Basin, which would provide both the nature and age of basin sediments imaged in seismic reflection data. At a larger scale, the timing of the opening of the Sea of Marmara along the NAF is constrained by the observation of a large anticline in the Dardanelles which was offset by the fault some 5 My ago [*Armijo et al.*, 1999], although the nature of the folding and the stratigraphy in this area have been disputed [*Yaltırak et al.*, 2000]. Present-day sedimentation rate in the central pull-apart of the Central Basin has been found to be as high as 3 mm/yr [*Armijo et al.*, 2005]. Therefore *Hirn et al.* [2002, 2003] suggested that pull-apart activity has been taking place in the Central Basin for about 1.5 My, on the basis of estimation of synkinematic sediment thickness of about 4.5 km. A similar calculation can be made for the Çınarcık Basin, assuming that this sedimentation rate is also valid, on average, for deposition of sediments in the Çınarcık Basin: a maximum sedimentary thickness of 5–6 km yields and age of 1.7–2 My for the basin. This figure, even very poorly constrained, is consistent with the westward propagation of the NAF, since the eastern Marmara Sea and especially the Çınarcık Basin likely started opening before the central part of the Marmara Sea. A tectonic model using GPS velocities suggests the present-day Anatolia/Eurasia motion is accommodated across the Marmara region by 18–20 mm/yr of right-lateral slip and 8 mm/yr of pure extension [*Flérit et al.*, 2003, 2004]. Furthermore, *Armijo et al.* [2002] gave a reconstruction for the past ~200,000 years by restoring a 3.5-km offset along the strike-slip fault segment connecting the Çınarcık and Central basins. It shows that the amount of north-south opening due to extensional motion is about 2 km in the Çınarcık Basin. Therefore assuming that the slip rate on the northern NAF (~20 mm/yr) has been fairly constant in the last few million years with a constant amount of partitioning, one requires 1.8 My to produce an 18-km wide basin (width measured in a N40° direction), if the basin-bounding faults are planar and there are no

block rotations. This figure is fully consistent with our estimation of 1.7 to 2 My from the total synkinematic sediment thickness.

6. Conclusion

[43] The Çınarcık Basin is an active transtensional basin along the northern NAF. Basin-bounding faults with significant extensional component of motion are imaged along both north and south sides of the basin. There is no indication in the data for a single throughgoing strike-slip fault, neither a cross-basin fault nor a pure strike-slip fault running along the northern margin. Results from the Leg 2 of the SEISMARMARA survey suggest that the Çınarcık Basin has a thick sediment fill, with a maximum sediment thickness of 6 km or more, though not uniformly distributed. In the eastern half of the basin, normal motion on the northern fault dominates (with a typical half-graben structure), whereas in the western half, dominant activity has switched onto the southern fault (with tilting of sediments toward the south and development of a subbasin). The area which seems to have opened most recently is the narrow, deepest part of the basin in the east. Overall, the Çınarcık Basin might be about 2 My old, but no reliable age constraint is available at the moment.

[44] There are few examples in the literature of dense seismic imaging of transtensional basins. The SEISMARMARA survey shows that the lateral variability of the fault system and sedimentary structure requires such densely spaced data to understand the formation of this type of basin.

[45] **Acknowledgments.** We thank the captain (H. Piton) and crew of R/V Le Nadir. The SEISMARMARA survey (2001) was carried out within a French-Turkish collaborative program on seismic risk in Istanbul and the Sea of Marmara, coordinated by INSU-CNRS and TUBITAK. We thank the Associate Editor and two reviewers (A. Okay and N. Seeber), who provided insightfull comments and constructive criticism on an earlier version of the manuscript. This is IPGP contribution number 2208.

References

Ambraseys, N. N., and C. F. Finkel (1991), Long-term seismicity of Istanbul and of the Marmara Sea region, *Terra Nova*, *3*, 527–539.

Ambraseys, N. N., and J. A. Jackson (2000), Seismicity of the Sea of Marmara (Turkey) since 1500, *Geophys. J. Int.*, *141*, F1–F6.

Armijo, R., B. Meyer, A. Hubert, and A. Barka (1999), Westward propagation of the North Anatolian Fault into the northern Aegean: Timing and kinematics, *Geology*, *27*, 267–270.

Armijo, R., B. Meyer, S. Navarro, G. King, and A. Barka (2002), Asymmetric slip partitioning in the Sea of Marmara pull-apart: A clue to propagation process of the North Anatolian Fault?, *Terra Nova*, *14*, 80–86.

Armijo, R., N. Pondard, B. Meyer, B. Mercier de Lépinay, and G. Uçarkus (2005), Submarine fault scarps in the Sea of Marmara pull-apart (North Anatolian Fault): Implications for seismic hazard in Istanbul, *Geochem. Geophys. Geosyst.*, *6*, Q06009, doi:10.1029/2004GC000896.

Ates, A., T. Kayiran, and I. Sincer (2003), Structural interpretation of the Marmara region, NW Turkey, from aeromagnetic, seismic and gravity data, *Tectonophysics*, *367*, 41–99.

Aydin, A., and A. Nur (1982), Evolution of pull-apart basins and their scale independence, *Tectonics*, *1*, 91–105.

Avedik, F., V. Renard, J. P. Allenou, and B. Morvan (1993), "Single-bubble" air-gun array for deep exploration, *Geophysics*, *8*, 366–382.

Barka, A., and K. Kadinsky-Cade (1988), Strike-slip fault geometry in Turkey and its influence on earthquake geometry, *Tectonics*, *7*, 663–684.

Basile, C., and J.-P. Brun (1999), Transtensional faulting patterns ranging from pull-apart basins to transform continental margins: An experimental investigation, *J. Struct. Geol.*, *21*, 23–37.

Bécel, A., et al. (2004), Seismic structure and activity of the North Anatolian Fault in the Sea of Marmara from the SEISMARMARA Leg 1 seismic survey, *Eos Trans. AGU*, *85*(47), Fall Meet. Suppl., Abstract S52A-04.

Ben-Avraham, Z., and M. D. Zoback (1992), Transform-normal extension and asymmetric basins: An alternative to pull-apart models, *Geology*, *20*, 423–426.

Bilham, R., and G. King (1989), The morphology of strike-slip faults: Examples from the San Andreas Fault, California, *J. Geophys. Res.*, *94*(B8), 10,204–10,216.

Çakir, Z., J.-B. de Chabalier, R. Armijo, B. Meyer, A. Barka, and G. Peltzer (2003), Coseismic and early post-seismic slip associated with the 1999 İzmit earthquake (Turkey), from SAR interferometry and tectonic field observations, *Geophys. J. Int.*, *155*, 93–110.

Çatagay, N., N. Görür, A. Algan, C. Eastoe, A. Tchapalyga, D. Ongan, T. Kuhn, and İ. Kuşçu (2000), Late Glacial-Holocene palaeoceanography of the Sea of Marmara: Timing of connections with the Mediterranean and the Black Seas, *Mar. Geol.*, *167*, 191–206.

Cetin, S., H. Carton, S. Singh, A. Hirn, B. de Voogd, M. Laigle, A. Bécel, R. Saatçilar, and S. Özalaybey (2003), Seismic evidence for a link between the Cinarcik Basin and the Central High in the Marmara Sea, in *Int. Symp. on the N. Anatolian, E. Anatolian and Dead Sea Fault Systems*, Middle East Technical University, Ankara.

Dessa, J.-X., H. Carton, and S. C. Singh (2005), 3D tomography of the Çınarcık Basin (Marmara Sea, Turkey) from ocean bottom recording of dense seismic profiles, *Geophys. Res. Abstr.*, *7*, Abstract EGU05-A-08303.

Dooley, T., and K. McClay (1997), Analog modeling of pull-apart basins, *AAPG Bull.*, *81*, 1804–1826.

Ergün, M., and E. Özel (1995), Structural relationship between the Sea of Marmara basin and the North Anatolian Fault zone, *Terra Nova*, *7*, 278–288.

Flérit, F., R. Armijo, G. C. P. King, B. Meyer, and A. Barka (2003), Slip partitioning in the Sea of Marmara pull-apart determined from GPS velocity vectors, *Geophys. J. Int.*, *154*, 1–7.

Flérit, F., R. Armijo, G. King, and B. Meyer (2004), The mechanical interaction between the propagating North Anatolian Fault and the back-arc extension in the Aegean, *Earth Planet. Sci. Lett.*, *224*, 347–362.

Garfunkel, Z. (1981), Internal structure of the Dead Sea leaky transform (rift) in relation to plate kinematics, *Tectonophysics*, *80*, 81–108.

Gölke, M., S. Cloetingh, and K. Fuchs (1994), Finite-element modeling of pull-apart basin formation, *Tectonophysics*, *240*, 45–57.

Hébert, H., F. Schindelé, Y. Altinok, B. Alpar, and C. Gazioğlu (2005), Tsunami hazard in the Marmara Sea (Turkey): A numerical approach to discuss active faulting and impact on the Istanbul coastal areas, *Mar. Geol.*, *215*, 23–43.

Hirn, A., S. Singh, R. Saatçılar, M. Laigle, B. deVoogd, A. Vigner, and T. Taymaz (2002), Reflection-seismic images and evolution at the scale of the crust and active faults of the Sea of Marmara Trough (SEISMARMARA 2001), *Geophys. Res. Abstr.*, *4*, Abstract EGS02-A-04792.

Hirn, A., et al. (2003), Elements of structure at crustal scale under the Sea of Marmara from multichannel seismics of the SEISMARMARA survey, *Geophys. Res. Abstr.*, *5*, Abstract EAE03-A-13126.

İmren, C., X. Le Pichon, C. Rangin, E. Demirbağ, B. Ecevitoğlu, and N. Görür (2001), The North Anatolian Fault within the Sea of Marmara: A new interpretation based on multi-channel seismic and multi-beam bathymetry data, *Earth Planet. Sci. Lett.*, *186*, 143–158.

Karabulut, H., M.-P. Bouin, M. Bouchon, M. Dietrich, C. Cornou, and M. Aktar (2002), The seismicity in the Eastern Marmara Sea after the 17 August 1999 İzmit earthquake, *Bull. Seismol. Soc. Am.*, *92*, 387–393.

Katzman, R., U. ten Brink, and J. Lin (1995), Three-dimensional modeling of pull-apart basins: Implications for the tectonics of the Dead Sea Basin, *J. Geophys. Res.*, *100*(B4), 6295–6312.

Le Pichon, X., et al. (2001), The active main Marmara fault, *Earth Planet. Sci. Lett.*, *192*, 596–616.

Mann, P., M. R. Hempton, D. C. Bradley, and K. Burke (1983), Development of pull-apart basins, *J. Geol.*, *91*, 529–554.

McClusky, S., et al. (2000), Global Positioning System constraints on the plate kinematics and dynamics in the eastern Mediterranean and Caucasus, *J. Geophys. Res.*, *105*, 5695–5719.

Muller, J., and A. Aydin (2005), Using mechanical modeling to constrain fault geometries proposed for the northern Marmara Sea, *J. Geophys. Res.*, *110*, B03407, doi:10.1029/2004JB003226.

Okay, A. I., A. Kaşhlar-Özcan, C. İmren, A. Boztepe-Güney, E. Demirbağ, and İ. Kuşçu (2000), Active faults and evolving strike-slip basins in the Sea of Marmara, northwest Turkey: A multichannel seismic reflection study, *Tectonophysics*, *321*, 189–218.

Özalaybey, S., M. Ergin, M. Aktar, C. Tapirdamaz, F. Biçmen, and A. Yörük (2002), The 1999 İzmit earthquake sequence in Turkey: Seismological and tectonic aspects, *Bull. Seismol. Soc. Am.*, *92*, 376–386.

Parke, J. R., T. A Minshull, G. Anderson, R. S. White, D. McKenzie, İ. Kuşçu, J. M. Bull, N. Görür, and C. Şengör (1999), Active faults

in the Sea of Marmara, western Turkey, imaged by seismic reflection profiles, *Terra Nova*, *11*, 223–227.

Parke, J. R., R. S. White, D. McKenzie, T. A. Minshull, J. M. Bull, İ. Kuşçu, N. Görür, and C. Şengör (2002), Interaction between faulting and sedimentation in the Sea of Marmara, western Turkey, *J. Geophys. Res.*, *107*(B11), 2286, doi:10.1029/2001JB000450.

Parke, J. R., R. S. White, D. McKenzie, T. A. Minshull, J. M. Bull, İ. Kuşçu, N. Görür, and C. Şengör (2003), The Sea of Marmara: A 2D seismic reflection profile data archive, *Geochem. Geophys. Geosyst.*, *4*(10), 1084, doi:10.1029/2002GC000493.

Parsons, T. (2004), Recalculated probability of M $\geq$ 7 earthquakes beneath the Sea of Marmara, Turkey, *J. Geophys. Res.*, *109*, B05304, doi:10.1029/2003JB002667.

Pondard, N., R. Armijo, G. King, B. Meyer, and F. Flérit (2007), Fault interactions in the Sea of Marmara pull-apart (North Anatolian Fault): Earthquake clustering and propagating earthquake sequences, *Geophys. J. Int.*, in press.

Rahe, B., D. A. Ferril, and A. P. Morris (1998), Physical analog modeling of pull-apart basin evolution, *Tectonophysics*, *285*, 21–40.

Rangin, C., X. Le Pichon, E. Demirbağ, and C. İmren (2004), Strain localization in the Sea of Marmara: Propagation of the North Anatolian Fault in a now inactive pull-apart, *Tectonics*, *23*, TC2014, doi:10.1029/2002TC001437.

Reilinger, R. E., et al. (2000), Coseismic and postseismic fault slip for the 17 August 1999, M = 7.5, Izmit, Turkey, earthquake, *Science*, *289*, 1519–1524.

Rodgers, D. A. (1980), Analysis of pull-apart basin development produced by an echelon strike-slip faults, in *Sedimentation in Oblique-Slip Mobile Zones*, edited by E. Ballance and H. G. Reading, pp. 27–41, *Spec. Publ. Int. Assoc. Sedimentol.*

Sato, T., J. Kasahara, T. Taymaz, M. Ito, A. Kamimura, T. Hayakawa, and O. Tan (2004), A study of microearthquake seismicity and focal mechanisms within the Sea of Marmara (NW Turkey) using ocean bottom seismometers (OBSs), *Tectonophysics*, *391*, 303–314.

Segall, P., and D. D. Pollard (1980), Mechanics of discontinuous faults, *J. Geophys. Res.*, *85*(B8), 4337–4350.

Smith, A. D., T. Taymaz, F. Oktay, H. Yüce, B. Alpar, H. Başaran, J. A. Jackson, S. Kara, and M. Şimşek (1995), High-resolution seismic profiling in the Sea of Marmara (northwest Turkey): Late Quaternary sedimentation and sea level changes, *Geol. Soc. Am. Bull.*, *107*(8), 923–936.

Stein, R. S., A. A. Barka, and J. H. Dieterich (1997), Progressive failure on the North Anatolian Fault since 1939 by earthquake stress triggering, *Geophys. J. Int.*, *128*, 594–604.

Taymaz, T., J. Jackson, and D. McKenzie (1991), Active tectonics of the north and central Aegean Sea, *Geophys. J. Int.*, *106*, 433–490.

Uçarkus, G., R. Armijo, N. Pondard, B. Meyer, and Z. Çakir (2006), The Eastern Marmara pull-apart junction (North Anatolian Fault) and its relation to the submarine end of the 1999 Izmit earthquake rupture, *Geophys. Res. Abstr.*, *8*, Abstract EGU06-A-08807.

Westaway, R. (1994), Present-day kinematics of the Middle-East and eastern Mediterranean, *J. Geophys. Res.*, *99*(B6), 12,071–12,090.

Wong, H. K., T. Lüdmann, A. Ulug, and N. Görür (1995), The Sea of Marmara: A plate boundary sea in an escape tectonic regime, *Tectonophysics*, *244*, 231–250.

Yaltırak, C., M. Sakınç, and F. Y. Oktay (2000), Westward propagation of the North Anatolian fault into the northern Aegean: Timing and kinematics, Comment, *Geology*, *28*, 187–188.

Zhang, P., B. C. Burchfiel, S. Chen, and Q. Deng (1989), Extinction of pull-apart basins, *Geology*, *17*, 814–817.

S. Bazin, H. Carton, A. Ricolleau, and S. C. Singh, Equipe de Géosciences Marines, Institut de Physique du Globe de Paris, 4 place Jussieu, 75005 Paris, France. (carton@ipgp.jussieu.fr)

S. Cetin, F. Karakoç, and V. Sevilgen, TUBITAK-MAM, Marmara Research Center, Gebze-Kocaeli, Turkey.

B. de Voogd, Département Sciences de la Terre, Université de Pau, Pau, France.

A. Hirn and A. Vigner, Equipe de Sismologie, Institut de Physique du Globe de Paris, Paris, France.

N. Oçakoğlu, Department of Geophysics, Istanbul Technical University, Istanbul, Turkey.